Earth Syst. Dynam. Discuss., 1, 325–355, 2010
www.earth-syst-dynam-discuss.net/1/325/2010/
doi:10.5194/esdd-1-325-2010

Earth System Dynamics Discussions

Entropy production and multiple equilibria: the case of the ice-albedo feedback

C. Herbert[1,2], **D. Paillard**[1], **and B. Dubrulle**[2]

[1]Laboratoire des Sciences du Climat et de l'Environnement, IPSL, CEA-CNRS-UVSQ, UMR 8212, Gif-sur-Yvette, France
[2]Service de Physique de l'Etat Condensé, DSM, CEA Saclay, CNRS URA 2464, Gif-sur-Yvette, France

Received: 5 October 2010 – Accepted: 13 October 2010 – Published: 19 October 2010

Correspondence to: C. Herbert (corentin.herbert@lsce.ipsl.fr)

Published by Copernicus Publications on behalf of the European Geosciences Union.

Abstract

Nonlinear feedbacks in the Earth System provide mechanisms that can prove very useful in understanding complex dynamics with relatively simple concepts. For example, the temperature and the ice cover of the planet are linked in a positive feedback which gives birth to multiple equilibria for some values of the solar constant: fully ice-covered Earth, ice-free Earth and an intermediate unstable solution. In this study, we show an analogy between a classical dynamical system approach to this problem and a Maximum Entropy Production (MEP) principle view, and we suggest a glimpse on how to reconcile MEP with the time evolution of a variable. It enables us in particular to resolve the question of the stability of the entropy production maxima. We also compare the surface heat flux obtained with MEP and with the bulk-aerodynamic formula.

1 Introduction

A very broad class of problems in climate modelling consists of studying the evolution of a particular field (e.g. surface temperature, precipitation, etc.) when an external parameter, or *forcing*, is varied. Most of the time the response to this variation is not linear. Feedbacks can amplify or damp the effect of the initial perturbation. One of these feedbacks aroused a proficient branch in scientific literature in the 70's, when Budyko and Sellers simultaneously suggested that the interaction between sea ice and climate could have dramatic consequences. Indeed, the higher the global temperature on Earth, the less the ice cover is likely to extend, and thus the lower the albedo. A lower albedo leads in turn to a higher global temperature, and so on and so forth until all the ice is melted. Stimulated by this pioneer work, the questions of the stability of the climate as well as the consequences such feedbacks might have for understanding paleoclimates were extensively studied, using the whole hierarchy of models, from the most simple Energy Balance Models (EBMs) to the complex General Circulation Models (GCMs).

ESDD

1, 325–355, 2010

Using 1-D EBMs, Budyko and Sellers had found two stable equilibrium positions for the edge of the ice cover, one corresponding to the present climate and one to a fully ice-covered Earth (Budyko, 1969; Sellers, 1969). A large part of the subsequent work was concerned with verifying that these results still held with various different versions of the Budyko-Sellers models, with different heat transport parameterizations, temperature dependance expressions in the planetary albedo, numerical schemes, ... (Faegre, 1972; Schneider and Gal-Chen, 1973; Held and Suarez, 1974; North, 1975a; Gal-Chen and Schneider, 1976, e.g.). Some elegant analytical solutions were found for these models (Chylek and Coakley, 1975; North, 1975a,b), and various mathematical methods were applied to determine the stability of the equilibria (Ghil, 1976; Su and Hsieh, 1976; Frederiksen, 1976; Cahalan and North, 1979; North et al., 1979). Owing to the extreme sensitivity of climate to variations in the solar constant found by the first studies, the precise position of the tipping point between present climate and a *deep freezed* Earth was of primary concern. Further investigation by Lian and Cess (1977) and Oerlemans and van den Dool (1978) revealed that the sensitivity was much less than initially thought. A fundamental question raised by these results was that of the *transitivity* of the climate system in Lorenz's terminology (Lorenz, 1968, 1970), and the difference between forced and free fluctuations (Schneider and Gal-Chen, 1973; Ghil, 1976; Fraedrich, 1978). For a comprehensive review of the various models, parameterizations and problems pertaining to Energy Balance Models and the ice-albedo feedback, the reader is referred to North et al. (1981).

In this contribution, we will first give a brief account of the reformulation of these questions with the vocabulary of dynamical system theory: how do multiple equilibria arise from the ice-albedo feedback, what does the bifurcation diagram look like, etc. The model used here is a two box energy balance model with a simplified radiative transfer using the Net Exchange Formulation (see e.g. Dufresne et al., 2005), and a bulk aerodynamic formula for the surface heat flux. In a second step, we draw an analogy between this dynamical system view and the results obtained when predicting the surface heat flux from the Maximum Entropy Production (MEP) principle. The MEP

ESDD
1, 325–355, 2010

principle, as originally expressed by Paltridge (1975, 1978, 1979) for the climate system, provides a variational principle to compute energy fluxes that are not otherwise constrained by the laws of physics. Originally, Paltridge and others applied MEP to the meridional energy transport (Paltridge, 1975, 1978; Grassl, 1981; Gerard et al., 1990; Lorenz et al., 2001, e.g.), but other studies (Schulman, 1977; Ozawa and Ohmura, 1997; Pujol and Fort, 2002) indicate that it may be valid on the vertical also.

As noticed by Oerlemans and van den Dool (1978), Crafoord and Källén (1978) and Fraedrich (1978), the fundamentally radiative nature of the bifurcation giving birth to multiple equilibria encourages one in thinking that a zero-dimensionnal model is sufficient to capture the structure of the mechanism while avoiding the use of more cumbersome mathematics (namely the Sturm-Liouville theory). Therefore we will restrict ourselves here to this idealized case. Note also that most of our work could be transposed easily to other feedbacks, like the water-vapour feedback.

2 The ice-albedo feedback, multiple equilibria and the hysteresis cycle: the dynamical system approach

2.1 A simple two-layer EBM using the net exchange formulation

We use a slightly different formulation of the model described in Herbert et al. (2010), as represented in Fig. 1. A grid cell is still characterized by a surface temperature T_g and an atmospheric temperature T_a, and we note Ψ_{gs}^{SW} (resp. Ψ_{as}^{SW}) the flux of solar energy received by the ground (resp. absorbed by the atmosphere). Ψ_{ag}^{IR} is the net energy exchange rate between the ground and the atmospheric column per unit surface (i.e. the greenhouse effect), and Ψ_{sa}^{IR} (resp. Ψ_{sg}^{IR}) is the cooling to space term for the atmosphere (resp. the surface). The net energy exchange rates per unit surface are expressed as functions of T_g and T_a as:

$$\Psi_{gs}^{SW} = (\bar{s}(\alpha) - s)(1 - \alpha)\, \xi\, S, \tag{1}$$

ESDD
1, 325–355, 2010

$$\Psi_{as}^{SW} = (s + \alpha\, s^*)\, \xi\, S, \quad (2)$$

$$\Psi_{ag}^{IR} = t\, \sigma\, T_g^4 - t\, \sigma\, T_a^4, \quad (3)$$

$$\Psi_{sa}^{IR} = t\, \sigma\, T_a^4, \quad (4)$$

$$\Psi_{sg}^{IR} = \left(1 - \frac{t}{\mu}\right) \sigma\, T_g^4, \quad (5)$$

where α is the surface albedo, $t,\ s,\ s^*,\ \bar{s}$ are radiative coefficients and μ is the Elsasser factor (see Herbert et al., 2010 for a derivation of the equations and a discussion of the coefficients).

In addition to radiation, energy is exchanged due to atmospheric and oceanic transport as well as sensible heat at the surface. Let us embed all of these energy transfer modes in two variables: *da* (resp. *dg*) represents the net convergence (the opposite of the divergence) of energy into the atmospheric cell (resp. surface layer). Writing ζ_a for the atmospheric convergence (this variable was designated by ζ in Herbert et al., 2010), ζ_o for the oceanic convergence (this was not taken into account in Herbert et al., 2010), and q for the surface heat flux, we have

$$da = \zeta_a + q, \quad (6)$$

$$dg = \zeta_o - q. \quad (7)$$

Knowing the convergence of energy in each cell – atmosphere or ground – it is in general not possible without further assumptions to separate the contribution due to surface fluxes, atmospheric transport, and oceanic transport when applicable. Of course, over land, it is reasonable to assume that *dg* is just the surface energy flux (i.e. $\zeta_o = 0$) , and then $da + dg$ is the convergence of energy due to the atmospheric flow.[1]

The energy balance equations for the atmosphere and the surface read

$$R_a\left(T_a, T_g\right) + da = 0, \quad (8)$$

[1] This will also be the case in the zero-dimensional model considered here: $da = -dg$ being the surface heat flux.

ESDD
1, 325–355, 2010

$$R_g\left(T_a, T_g\right) + dg = 0, \quad (9)$$

where

$$R_a\left(T_a, T_g\right) = \Psi_{as}^{SW} + \Psi_{ag}^{IR} - \Psi_{sa}^{IR} = (s + \alpha s^*)\,\xi\,S + t\left(\sigma T_g^4 - 2\sigma T_a^4\right), \quad (10)$$

$$R_g\left(T_a, T_g\right) = \Psi_{gs}^{SW} - \Psi_{ag}^{IR} - \Psi_{sg}^{IR} = (\bar{s} - s)(1 - \alpha)\,\xi\,S - t\left(\sigma T_g^4 - \sigma T_a^4\right) \quad (11)$$

$$- \left(1 - \frac{t}{\mu}\right)\sigma T_g^4.$$

2.2 The zero-dimensional model with bulk aerodynamic formula

In the case of a zero-dimensional, two-layer model considered here for simplicity, the net convergence of energy in the atmospheric box (i.e. the divergence of the diabatic heating at the surface, $da = q = -dg$) can be simply interpreted as the surface heat flux. In this section, we adopt an aerodynamic bulk formula (Peixoto and Oort, 1992) to express this flux as a function of the temperatures T_a and T_g:

$$da = q_{baf}\left(T_a, T_g\right) = c_{pa}\,C_D\,u_s\left(T_g - T_a\right). \quad (12)$$

Now the model can be seen as a two-dimensional dynamical system:

$$\begin{pmatrix} \dot{T}_a \\ \dot{T}_g \end{pmatrix} = F\left(T_a, T_g\right), \quad (13)$$

with

$$F\left(T_a, T_g\right) = \begin{pmatrix} F_1\left(T_a, T_g\right) \\ F_2\left(T_a, T_g\right) \end{pmatrix}, \quad (14)$$

ESDD

1, 325–355, 2010

and

$$F_1\left(T_a, T_g\right) = \frac{1}{c_{pa}}\left(R_a\left(T_a, T_g\right) + q_{baf}\left(T_a, T_g\right)\right), \tag{15}$$

$$F_2\left(T_a, T_g\right) = \frac{1}{c_{pg}}\left(R_g\left(T_a, T_g\right) - q_{baf}\left(T_a, T_g\right)\right). \tag{16}$$

Our main interest here is to find the equilibrium positions of the system, i.e. the fixed points of the dynamical system, given by the roots of F, and to study their stability. Of course, the dynamics of a two-dimensional dynamical system can be more complex than just a relaxation to an equilibrium position (although it is still rather gentle, see Guckenheimer and Holmes, 1983, for example), contrary to one-dimensional dynamical systems. Still, let us note here that the first equation in $F\left(T_a, T_g\right) = 0$ can be solved algebraically in T_a to obtain a relation $T_a^* = f\left(T_g^*\right)$ where $\left(T_a^*, T_g^*\right)$ is a fixed point of the system. Thus the number of fixed points of the two-dimensional system is exactly the number of roots of the scalar equation $F_2\left(f\left(T_g\right), T_g\right) = 0$.

For simplicity, we will consider here the projection of the dynamical system (Eq. 16) onto the T_g axis:

$$\dot{T}_g = F_2\left(f\left(T_g\right), T_g\right). \tag{17}$$

As just explained, this dynamical system, although not mathematically equivalent to the full dynamical system (Eq. 14), has the same equilibrium positions. Physically, this simplification is motivated by the fact that the atmosphere can be assumed to reach equilibrium very quickly, hence the evolution of T_a is enslaved by the dynamics of T_g. In other words, the system (Eq. 17) is just the system (Eq. 14) with $c_{pa} = 0$.

2.3 Multiple equilibria

The values of the coefficients used here are reproduced in Table 1. Taking for the albedo the fixed value $\alpha_0 = 0.15$, the system only has one fixed point, as plotting the

ESDD
1, 325–355, 2010

function $F_2\left(f\left(T_g\right), T_g\right) = 0$ clearly shows (see Fig. 2). In this case, the equilibrium is at a global mean surface temperature of $T_g^0 \approx 288\,\text{K}$.

But in reality, the higher the global mean temperature, the lower the extent of the regions that can sustain an ice-cover. This positive feedback can be encoded in the following temperature dependance for the albedo :

$$\alpha\left(T_g\right) = \alpha_F + \frac{(\alpha_I - \alpha_F)}{2}\left(1 + \tanh\left(\frac{T_0 - T_g}{\Delta T}\right)\right), \tag{18}$$

where α_F (resp. α_I) represents the value of the planetary albedo over an ice-free (resp. fully ice-covered) area, and T_0 and ΔT are parameters determining the transition from ice-free to ice-covered conditions. One could simply use a step function between ice-free and ice-covered albedo values, or a piecewise linear function, but we choose this expression because it depends smoothly on the temperature.

Replacing α in Eq. (14) with Eq. (18) yields a new dynamical system

$$\begin{pmatrix} \dot{T}_a \\ \dot{T}_g \end{pmatrix} = G\left(T_a, T_g\right), \tag{19}$$

where the fixed points are again determined by the conditions, g being defined similarly to f (or obtained by substitution of the albedo function into f),

$$T_a^* = g\left(T_g^*\right), \tag{20}$$

$$0 = G_2\left(g\left(T_g^*\right), T_g^*\right). \tag{21}$$

Plotting the curve $G_2\left(g\left(T_g\right), T_g\right)$ as a function of T_g (Fig. 3) shows that for certain values of the solar constant, three solutions coexist. This range can be determined to be approximately $0.98\,S_0 \leq S \leq 1.08\,S_0$. Outside this range, only one solution subsists. For the present value of the solar constant, $S = S_0$, for instance, these equilibria correspond to a fully glaciated Earth (*snowball* state) $T_g^S \approx 249\,\text{K}$, an ice-free Earth

ESDD
1, 325–355, 2010

$T_g^P \approx 287$ K which can be identified with the present climate, and an intermediate glacial state $T_g^G \approx 275$ K. For a low value of the solar constant (e.g. $0.95\,S_0$), only the snowball state T_g^S subsists. Similarly, at high solar constant (e.g. $1.1\,S_0$), the only equilibrium is found on the ice-free branch T_g^P.

A fixed point X^* of the dynamical system $\dot{X} = F(X)$ is said to be (linearly) stable if all the eigenvalues of the jacobian of F are negative (see Arnold, 1984 for a complete classification of the two-dimensional fixed points). In this model we find that T_g^P and T_g^S are always stable nodes when they exist, while T_g^G is a saddle-point.

The stability can also be read directly on Fig. 3 for the 1-D-reduced system: stable equilibria correspond to roots of the function with negative derivative, while at the unstable equilibrium, the curve crosses the x-axis with an upward slope.

Summarizing the above results, Fig. 4 represents the curve of the fixed points when sweeping a large range of values for S : it is the bifurcation diagram of the dynamical system. Creation of a pair of stable/unstable equilibria at the tipping points $0.98\,S_0$ and $1.08\,S_0$ is called a *saddle-node bifurcation*. Thus the hysteresis curve obtained for the temperature stems from the bifurcation structure of the dynamical system as two back-to-back saddle-node bifurcations. It is noteworthy that this figure does not depend upon the particular coefficients choice in the bulk formula, nor on the greenhouse effect. Would we set $q_{\text{baf}} = 0$ (radiative equilibrium with greenhouse effect) or/and $t = 0$ (greenhouse effect shut down), the hysteresis curve would remain qualitatively the same.

2.4 Potential for the dynamical system

The full two-variables dynamical system (Eq. 13) cannot be expressed as the gradient of a potential function, but its one-dimensional projection can, like any other one-dimensional dynamical system. Let us thus introduce the potential V (defined up to an additive constant) such that

ESDD

1, 325–355, 2010

$$\dot{T}_g = -\frac{\partial V}{\partial T_g}. \quad (22)$$

Fixed points of this dynamical system correspond to critical points (i.e. extrema in this 1-D case) of the potential. The stability criterion becomes that stable fixed points are minima of the potential:

$$-\frac{\partial^2 V}{\partial T_g^2} < 0, \quad (23)$$

while its maxima are unstable fixed points.

Figure 5 shows the shape of the potential for different values of the solar constant. At low solar constant (e.g. $0.95\,S_0$), the potential has only one critical point, a minimum at $T \approx 245$ K. Increasing the value of the solar constant levels down the potential curve, until a second local minimum appears (along with a local maximum) with T above the freezing point, around $S \approx 0.98\,S_0$. At $S = S_0$, it is clear that the potential has two minima at $T \approx 250$ K and $T \approx 290$ K and a maximum at $T \approx 275$ K. Further increase of the solar constant leads to a deeper minimum at $T > 0\,^\circ$C while the minimum at $T < 0\,^\circ$C becomes shallower. Around $S \approx 1.08\,S_0$, the minimum at $T < 0\,^\circ$C disappears (it annihilates with the local maximum); for $S = 1.1\,S_0$, the only minimum is found at $T \approx 300$ K.

Note that, as expected, the critical points of the potential obtained for the three values of the solar constant considered here match with the values of Fig. 3. Also, the number of critical points of the potential changes at the bifurcation points of the dynamical system.

ESDD
1, 325–355, 2010

3 The entropy production rate and the ice-albedo feedback

In this section, we do not use anymore the bulk aerodynamic formula for the surface flux $da = -dg$, but the Maximum Entropy Production Principle, as described in Herbert et al. (2010).

3.1 The entropy production rate in zero-dimensions

Let us consider the model of Sect. 2.1 and introduce the entropy production rate per unit surface

$$\dot{S} = \frac{da}{T_a} + \frac{dg}{T_g}. \tag{24}$$

Substituting Eqs. (8)–(9) into Eq. (24) for da and dg, $\dot{S}$ can be considered as a functional of the temperature field. We are looking for its maxima subject to the constraint

$$da + dg = 0. \tag{25}$$

The sum of Eqs. (8) and (9) can thus be solved for T_a as a function of T_g, and the entropy production rate $\dot{S}$ is simply a function of one variable. Its graphical representation for the set of parameters given in Table 1 (fixed albedo α_0) is shown in Fig. 6. It is clear that there is only one local maximum, corresponding to a surface temperature $T_g \approx 22\,^{\circ}\mathrm{C}$.

Now, replacing in the equations the constant albedo α_0 by the temperature-dependent albedo (Eq. 18), the resulting entropy production rate curve is plotted in Fig. 7 for different values of the solar constant.

Unlike the potential for the dynamical system in Sect. 2.4, the entropy production rate always has at least two local maxima and a local minimum. In fact, over a rather narrow range, estimated to be $0.95\,S_0 \le S \le 1.005\,S_0$, the entropy production rate even has three maxima and two minima. This is even clearer on the contour plot of the entropy production rate as a function of T_g and S/S_0 (Fig. 8). Hence, there is indeed

ESDD
1, 325–355, 2010

an analogue of the *fold* of the potential in the classical dynamical picture in the context of the entropy production surface, but the values a which it takes place do not exactly correspond.

Besides, a large portion of the curve on Fig. 7 lies under the abscissa axis: for the corresponding range of temperature values, the entropy production rate is negative, contrary to what the second law of thermodynamics states (or more precisely its extension to non-equilibrium systems). It seems reasonable to impose the condition

$$\dot{S}\left(T_g\right) \geq 0, \tag{26}$$

thereby restricting the range of values T_g can actually take. In this case, this is equivalent to requiring that the surface heat flux goes from hot to cold. With this additional constraint, the range of possible values of the solar constant allowing for coexistence of multiple equilibria (two or three) can be determined approximately: $0.8\,S_0 \leq S \leq 1.124\,S_0$.

Note that the entropy production rate on the *snowball* state (the lower branch on Fig. 8) is a flat function of the solar constant, whereas it is an increasing function under warm climates (upper branch on Fig. 8). This is in accordance with Fig. 4a of Lucarini et al. (2010) who computed the entropy production rate, together with other thermodynamics quantities like irreversibility and efficiency, as diagnostic tools for both warm climate and snowball Earth in the model of intermediate complexity PLASIM (Fraedrich et al., 2005).

3.2 Stability of the MEP states

Figure 8 constitutes the analogue of the hysteresis diagram of Fig. 4 in the MEP framework, with two branches of equilibria corresponding to ice-free and snowball Earth states connected by an intermediate equilibrium. But the question of the stability of these equilibria cannot be addressed in this context. Indeed, $-\dot{S}$ is by no means a potential for the dynamical system, even though we claim that its minima correspond

ESDD
1, 325–355, 2010

to equilibrium points: the dynamics of the system is given by the first law of thermodynamics. Here, it reads

$$c_{pa} \frac{dT_a}{dt} = R_a \left(T_a, T_g\right) + da, \tag{27}$$

$$c_{pg} \frac{dT_g}{dt} = R_g \left(T_a, T_g\right) + dg. \tag{28}$$

We suggest here that the time derivative in these equations can be treated as a flux. Therefore we can apply MEP to the problem of the time evolving system just by considering the time dimension as a geometric dimension (see Fig. 9). In other words, the system becomes a 1 (time) + 0.5 (space, simplified vertical dimension) dimension model.

More explicitly, let T_a^0, T_a^1, T_g^0, T_g^1 be respectively the air temperature at time t and $t+dt$ and the surface temperature at time t and $t+dt$. Remembering that here, $da = q = -dg$, we can write the instantaneous entropy production rate as

$$\delta \dot{S}\left(T_a^1, T_g^1\right) = da\left(\frac{1}{T_a^1} - \frac{1}{T_g^1}\right) = \left(R_g\left(T_a^1, T_g^1\right) - c_{pg}\frac{T_g^1 - T_g^0}{dt}\right)\left(\frac{1}{T_a^1} - \frac{1}{T_g^1}\right). \tag{29}$$

Summing Eqs. (27) and (28), we can also express T_a^1 as a function of T_a^0, T_g^0 and T_g^1. Knowing T_a^0 and T_g^0, we can thus compute the maximum of the function $\delta\dot{S}$ as a function of T_g^1 only, deduce T_a^1 and iterate the same process over again. The trajectory obtained with this scheme maximizes the instantaneous entropy production rate, starting from a given initial condition.

Integrating the system with this method, initialized in the vicinity of the different maxima of the entropy production rate at steady-state, provides an answer to the question of stability: it is found here that the warm branch as well as the snowball branch of Fig. 8 are stable, while the intermediate branch is unstable. The maxima of the entropy production and their stability are plotted as functions of the solar constant on Fig. 10,

ESDD
1, 325–355, 2010

Title Page
Abstract | Introduction
Conclusions | References
Tables | Figures
◂◂ | ▸▸
◂ | ▸
Back | Close
Full Screen / Esc
Printer-friendly Version
Interactive Discussion

analogously to Fig. 4. This result draws the final line in the parallel between the dynamical system approach and the MEP approach. Note that the limits of this analogy are reached at some points: Fig. 10 cannot be considered as a usual bifurcation diagram. As a consequence, the lines of existence of the maxima need not depend continuously on the parameter, and for certain values of the parameter (for example $S \approx 0.9\,S_0$), two stable maxima coexist with no *unstable manifold* to separate them.

3.3 Surface heat flux and Snowball Earth deglaciation

In the case of the first section, the surface heat flux is parameterized as a function of T_a and T_g. As a consequence of this strong constraint, one could draw a bifurcation diagram for q_{baf} very similar to Fig. 4, with relatively weak surface heat flux q_{baf}^S for low solar constants (around $20\,W\,m^{-2}$), strong surface heat flux q_{baf}^P at high solar constants (around $100\,W\,m^{-2}$), with an unstable branch q_{baf}^G linking the two.

On the contrary, the surface heat flux obtained through the MEP procedure q_{mep} is much less constrained by the temperature gradient. Figure 11 shows the surface heat flux as a function of the temperature gradient $T_g - T_a$ for both cases: q_{baf} and q_{mep}. It is clear that the two differ completely, not only because the temperature gradients in the different climates are very different, but also because the shape of q_{mep} as a function of the temperature gradient is far from linear. Note that in the MEP snowball state, although the temperature gradient is relatively high, the surface flux remains very low. On the warm branch for the MEP state, high values of q_{mep} are obtained for high values of the solar constant. Hence, decreasing the solar constant brings the surface flux down, until the point where only the snowball state survives, with a similar low value of the surface heat flux.

This discrepancy between the two graphs is likely to be significant: it has been suggested that the suppression of the vertical temperature gradient in the snowball state numbers amongst the reasons that make deglaciation of the snowball Earth so difficult (Pierrehumbert, 2004, 2005; le Hir et al., 2010). Indeed, the temperature inversion

ESDD
1, 325–355, 2010

isolates the surface from all the forms of energy exchange: the greenhouse effect can only warm the surface when the air aloft is colder, latent heat plays a very limited role in this very dry atmosphere, and the sensible heat flux is also restricted by the vertical structure of the atmosphere. Pierrehumbert (2004) points out that a crucial role may be played by the surface fluxes parameterization and the convection parameterization. Here the simplicity of the model does not allow us to discuss the static stability, nor to come up with a clear explanation of the questioning Fig. 11, but it does certainly reinforce the idea that surface heat fluxes parameterization can play critical parts on important paleoclimate problems. In the case of the MEP surface heat flux, our results tend to indicate that it would be possible for the snowball earth to withstand a vertical temperature gradient higher than expected with very little loss in the form of sensible heat, thereby damaging the thermal shield of the surface layer mentioned above.

On a similar note, Lucarini et al. (2010) performed a thorough investigation of the thermodynamic properties of the snowball Earth as compared to warm climates, using the formalism of non-equilibrium thermodynamics applied to the climate system as described in Lucarini (2009). Computation of the thermodynamics efficiency, irreversibility and material entropy production clearly characterizes distinct thermodynamic regimes for the snowball Earth and ice-free climate. Our remarks about the surface heat flux in snowball conditions add up to their thermodynamic analysis.

4 Conclusions

The analogy developed in this study leads to some enlightening conclusions. First, about the ice-albedo feedback in itself, it provides a variational principle different from those previously suggested, with a thermodynamic motivation. On the contrary, all the candidates for variational formulations of the problem examined previously were rather ad hoc potentials for the dynamical system. The parallel between potentials properly speaking, which fully describe the dynamics of the system, and the entropy production rate, which only characterize equilibrium states, was pushed one step further with the

ESDD
1, 325–355, 2010
Entropy production and the ice-albedo feedback
C. Herbert et al.

introduction of a method to integrate a trajectory using the MEP principle. In particular we have shown that this method predicts the correct stability for the MEP predicted equilibria. We also investigated the behaviour of the surface heat flux in the snowball state. The results hint that MEP might prove useful in such extreme situations where the usual parameterizations face important difficulties. However, the highly simplified model considered here does not allow us to conclude against or in favour of the MEP parameterization, as compared to the bulk-aerodynamic formula.

As far as the MEP conjecture is concerned, our work adds up to the relatively short list of efforts up to now (essentially Shimokawa and Ozawa, 2002 and Jupp and Cox, 2010) to sort out how the principle should be understood in the presence of multiple entropy production maxima. These grounds, which are just starting to be explored, are bound to bear fruits both on theoretical and practical sides.

cnrs INSU
Institut national des sciences de l'Univers

The publication of this article is financed by CNRS-INSU.

References

Arnold, V.: Ordinary Differential Equations, Springer, New York, 1984. 333

Budyko, M.: The effect of solar radiation variations on the climate of the Earth, Tellus, 21, 611–619, 1969. 327

Cahalan, R. and North, G.: A Stability Theorem for Energy-Balance Climate Models, J. Atmos. Sci., 36, 1178–1188, 1979. 327

Chylek, P. and Coakley, J.: Analytical analysis of a Budyko-type climate model, J. Atmos. Sci., 32, 675–679, 1975. 327

Crafoord, C. and Källén, E.: A Note on the Condition for Existence of More than One Steady-State Solution in Budyko-Sellers Type Models, J. Atmos. Sci., 35, 1123–1124, 1978. 328

Dufresne, J., Fournier, R., Hourdin, C., and Hourdin, F.: Net exchange reformulation of radiative transfer in the CO_2 15 µm band on Mars, J. Atmos. Sci., 62, 3303–3319, 2005. 327

Faegre, A.: An intransitive model of the Earth-atmosphere-ocean system, J. Appl. Meteorol., 11, 4–6, 1972. 327

Fraedrich, K.: Structural and stochastic analysis of a zero-dimensional climate system, Q. J. Roy. Meteorol. Soc., 104, 461–474, 1978. 327, 328

Fraedrich, K., Jansen, H., Kirk, E., Luksch, U., and Lunkeit, F.: The Planet Simulator: Towards a user friendly model, Meteorol. Z., 14, 299–304, 2005. 336

Frederiksen, J.: Nonlinear albedo-temperature coupling in climate models, J. Atmos. Sci., 33, 2267–2272, 1976. 327

Gal-Chen, T. and Schneider, S.: Energy balance climate modeling: Comparison of radiative and dynamic feedback mechanisms, Tellus, 28, 108–121, 1976. 327

Gerard, J., Delcourt, D., and Francois, L.: The maximum entropy production principle in climate models: application to the faint young sun paradox, Q. J. Roy. Meteorol. Soc., 116, 1123–1132, 1990. 328

Ghil, M.: Climate stability for a Sellers-type model, J. Atmos. Sci., 33, 3–20, 1976. 327

Grassl, H.: The climate at maximum entropy production by meridional atmospheric and oceanic heat fluxes, Q. J. Roy. Meteorol. Soc., 107, 153–166, 1981. 328

Guckenheimer, J. and Holmes, P.: Nonlinear Oscillations, Dynamical Systems, and Bifurcations of Vector Fields, vol. 42 of Applied Mathematical Sciences, Springer, New York, 1983. 331

Held, I. and Suarez, M.: Simple albedo feedback models of the icecaps, Tellus, 26, 613–629, 1974. 327

Herbert, C., Paillard, D., Kageyama, M., and Dubrulle, B.: Present and Last Glacial Maximum climates as maximum entropy production states, Q. J. Roy. Meteorol. Soc., submitted, 2010. 328, 329, 335, 345

Jupp, T. E. and Cox, P.: MEP and planetary climates: insights from a two-box climate model containing atmospheric dynamics, Philos. T. Roy. Soc. B, 365, 1355–1365, 2010. 340

le Hir, G., Donnadieu, Y., Krinner, G., and Ramstein, G.: Toward the snowball earth deglaciation, Clim. Dynam., 35, 285–297, 2010. 338

Lian, M. and Cess, R.: Energy balance climate models: A reappraisal of ice-albedo feedback, J. Atmos. Sci., 34, 1058–1062, 1977. 327

ESDD

1, 325–355, 2010

Entropy production and the ice-albedo feedback

C. Herbert et al.

Lorenz, E. N.: Climatic determinism, Meteor. Mon., 8, 1–3, 1968. 327
Lorenz, E. N.: Climatic change as a mathematical problem, J. Appl. Meteorol., 9, 325–329, 1970. 327
Lorenz, R., Lunine, J., Withers, P., and McKay, C.: Titan, Mars and Earth: Entropy production by latitudinal heat transport, Geophys. Res. Lett., 28, 415–418, 2001. 328
Lucarini, V.: Thermodynamic efficiency and entropy production in the climate system, Phys. Rev. E, 80, 021118, doi:10.1103/PhysRevE.80.021118, 2009. 339
Lucarini, V., Fraedrich, K., and Lunkeit, F.: Thermodynamic analysis of snowball Earth hysteresis experiment: Efficiency, entropy production and irreversibility, Q. J. Roy. Meteorol. Soc., 136, 2–11, 2010. 336, 339
North, G.: Analytical solution to a simple climate model with diffusive heat transport, J. Atmos. Sci., 32, 1301–1307, 1975a. 327
North, G.: Theory of energy-balance climate models, J. Atmos. Sci., 32, 2033–2043, 1975b. 327
North, G., Howard, L., Pollard, D., and Wielicki, B.: Variational formulation of Budyko-Sellers climate models, J. Atmos. Sci., 36, 255–259, 1979. 327
North, G., Cahalan, R., and Coakley, J.: Energy Balance Climate Models, Rev. Geophy. Space Ge., 19, 91–121, 1981. 327
Oerlemans, J. and van den Dool, H.: Energy balance climate models: Stability experiments with a refined albedo and updated coefficients for infrared emission, J. Atmos. Sci., 35, 371–381, 1978. 327, 328
Ozawa, H. and Ohmura, A.: Thermodynamics of a global-mean state of the atmosphere – a state of maximum entropy increase, J. Climate, 10, 441–445, 1997. 328
Paltridge, G.: Global dynamics and climate-a system of minimum entropy exchange, Q. J. Roy. Meteorol. Soc., 101, 475–484, 1975. 328
Paltridge, G.: The steady-state format of global climate, Q. J. Roy. Meteorol. Soc., 104, 927–945, 1978. 328
Paltridge, G.: Climate and thermodynamic systems of maximum dissipation, Nature, 279, 630–631, 1979. 328
Peixoto, J. P. and Oort, A. H.: Physics of Climate, Springer, New York, 1992. 330
Pierrehumbert, R.: High levels of atmospheric carbon dioxide necessary for the termination of global glaciation, Nature, 429, 646–649, 2004. 338, 339

ESDD
1, 325–355, 2010

Pierrehumbert, R.: Climate dynamics of a hard snowball Earth, J. Geophys. Res., 110, D01111, doi:10.1029/2004JD005162, 2005. 338
Pujol, T. and Fort, J.: States of maximum entropy production in a one-dimensional vertical model with convective adjustment, Tellus, 54, 363–369, 2002. 328
Schneider, S. and Gal-Chen, T.: Numerical experiments in climate stability, J. Geophys. Res., 78, 6182–6194, 1973. 327
Schulman, L.: A theoretical study of the efficiency of the general circulation, J. Atmos. Sci., 34, 559–580, 1977. 328
Sellers, W.: A global climatic model based on the energy balance of the earth-atmosphere system, J. Appl. Meteorol., 8, 392–400, 1969. 327
Shimokawa, S. and Ozawa, H.: On the thermodynamics of the oceanic general circulation: Irreversible transition to a state with higher rate of entropy production, Q. J. Roy. Meteorol. Soc., 128, 2115–2128, 2002. 340
Su, C. and Hsieh, D.: Stability of the Budyko climate model, J. Atmos. Sci., 33, 2273–2275, 1976. 327

ESDD
1, 325–355, 2010

Entropy production and the ice-albedo feedback

C. Herbert et al.

Table 1. Values for the parameters of the 0D model (radiative coefficients, bulk aerodynamic formula parameters and ice-albedo feedback parameterization)

Symbol	μ	ξ	t	s	s^*	$\bar{s}$	α_0	S_0
Value	0.6	0.25	0.44	0.19	0.015	0.89	0.15	$1368\,W\,m^{-2}$
Symbol	C_D	u_s	c_{pa}	c_{pg}	α_I	α_F	T_0	ΔT
Value	0.008	$6\,m\,s^{-1}$	$1\,MJ\,K^{-1}\,m^{-2}$	$1.44\,MJ\,K^{-1}\,m^{-2}$	0.08	0.68	273.15 K	15 K

ESDD
1, 325–355, 2010

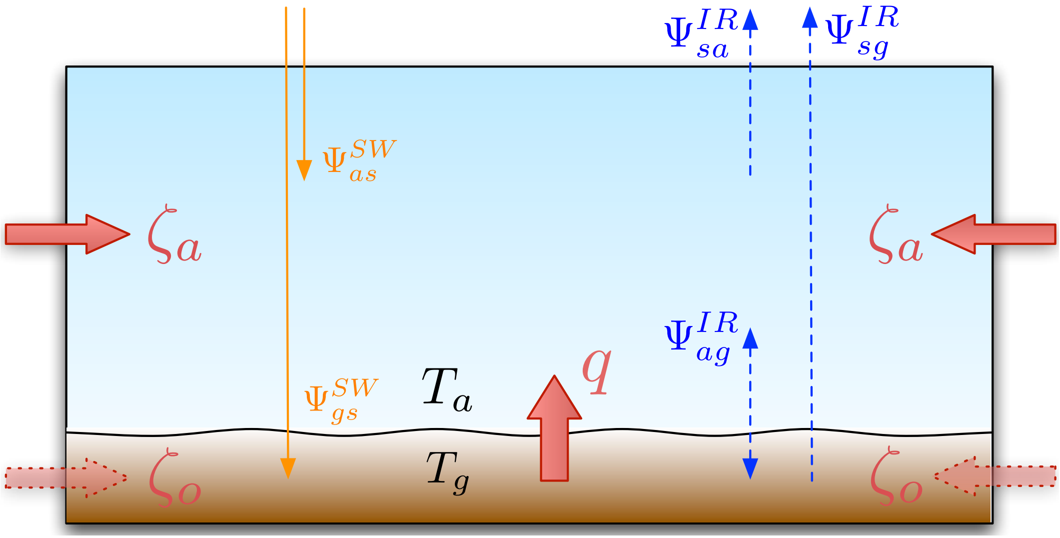

Fig. 1. A grid cell of the model, adapted from Herbert et al. (2010). Ψ^{ν}_{ij} are the energy exchange rates per unit surface due to radiative transfer (see text), q is the surface heat flux and ζ_a is the atmospheric energy convergence. Over the oceans, there is also an oceanic energy convergence ζ_o.

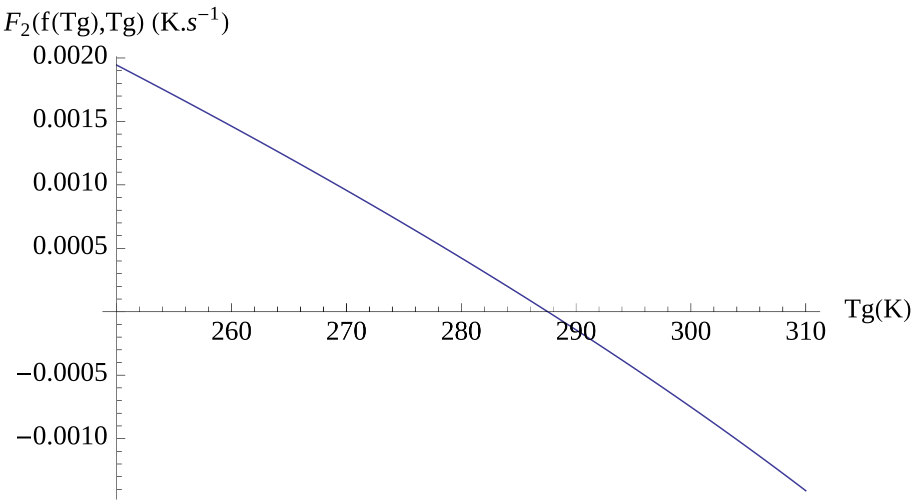

Fig. 2. Function $F_2\left(f(T_g),T_g\right)$ as a function of T_g (see text) with a fixed albedo has only one root.

ESDD
1, 325–355, 2010

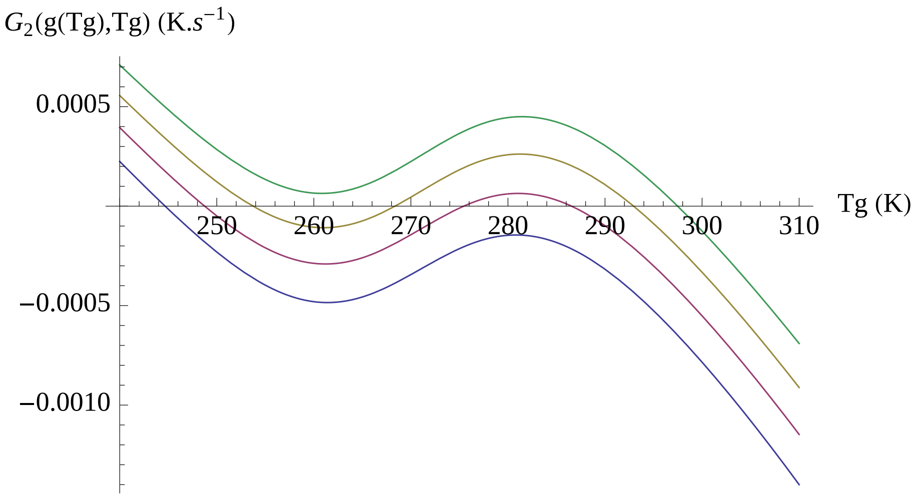

Fig. 3. Function $G_2\left(g(T_g),T_g\right)$ as a function of T_g (see text) including the ice-albedo feedback for different values of the solar constant: $0.95\,S_0$ (blue), S_0 (red), $1.05\,S_0$ (yellow), $1.1\,S_0$ (green).

ESDD
1, 325–355, 2010

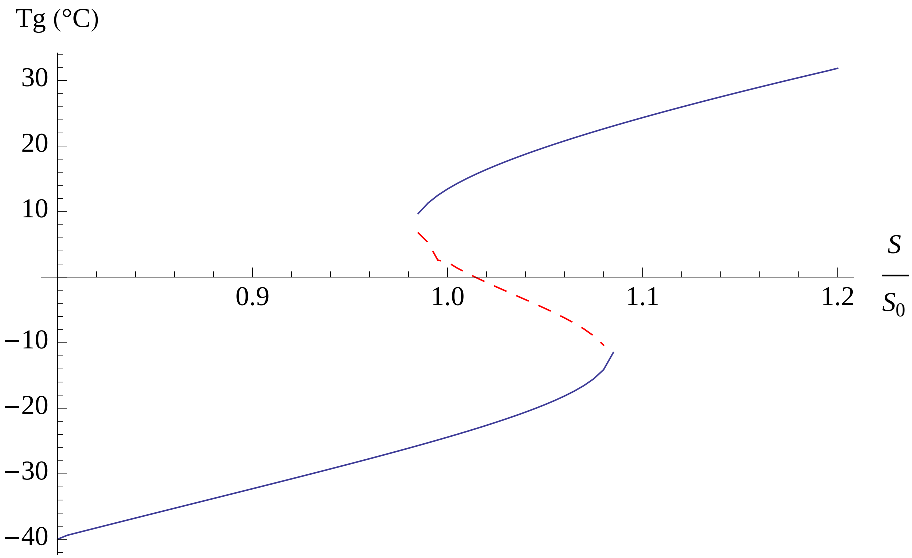

Fig. 4. Bifurcation diagram of the bulk aerodynamic formula model. T_g, T_P and T_S are plotted against S/S_0 when they exist. Stable fixed points are plotted in blue while the unstable solution is in dotted red. This figure clearly shows that two saddle-node bifurcations occur at respectively $S \approx 0.98\,S_0$ and $S \approx 1.08\,S_0$.

ESDD
1, 325–355, 2010

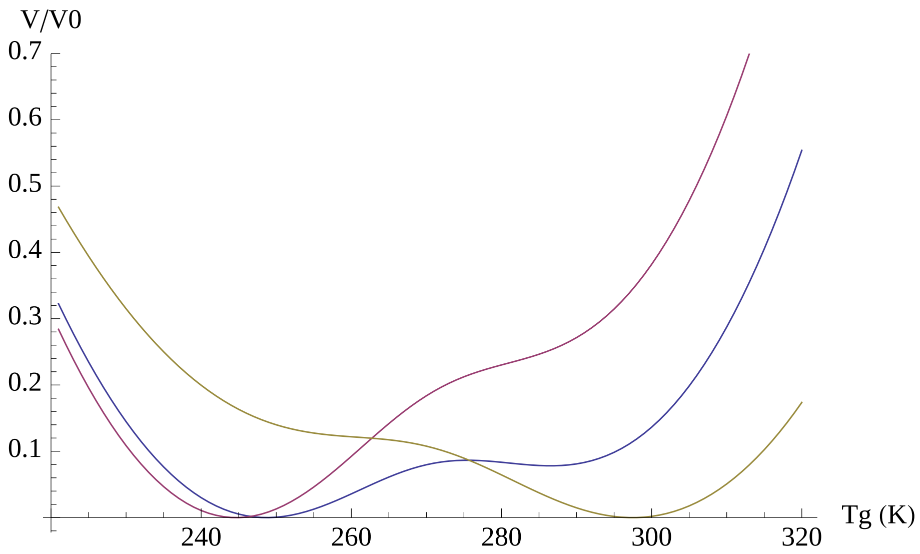

Fig. 5. Potential V (normalized) as a function of temperature T_g (in K) for three different values of the solar constant: $0.95\,S_0$ (red), S_0 (blue) and $1.1\,S_0$ (yellow). For the present value of the solar constant, the potential has a double well shape, with two stable equilibria, while for the two other values, the potential has only one minimum.

ESDD
1, 325–355, 2010

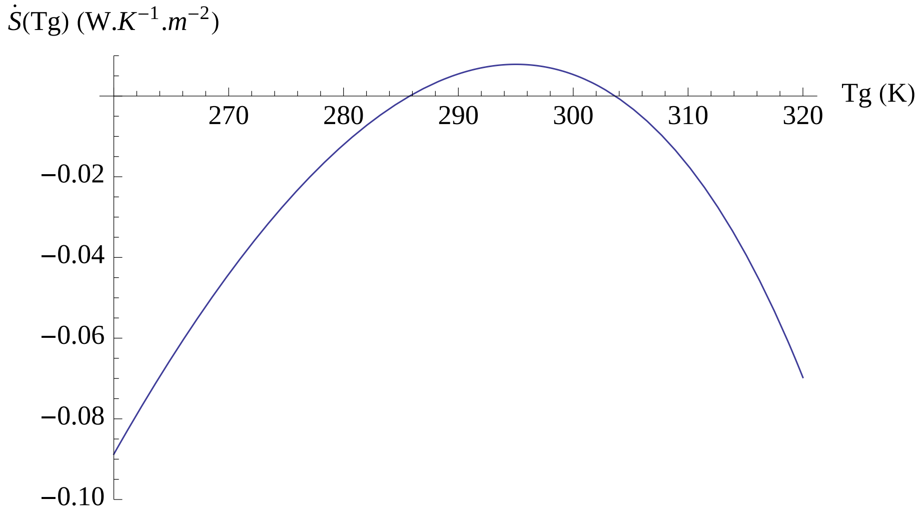

Fig. 6. Entropy production rate as a function of the surface temperature T_g for the 0D model at $S = S_0$. The only local maximum corresponds to $T_g \approx 22\,^{\circ}$C.

ESDD
1, 325–355, 2010

Entropy production and the ice-albedo feedback

C. Herbert et al.

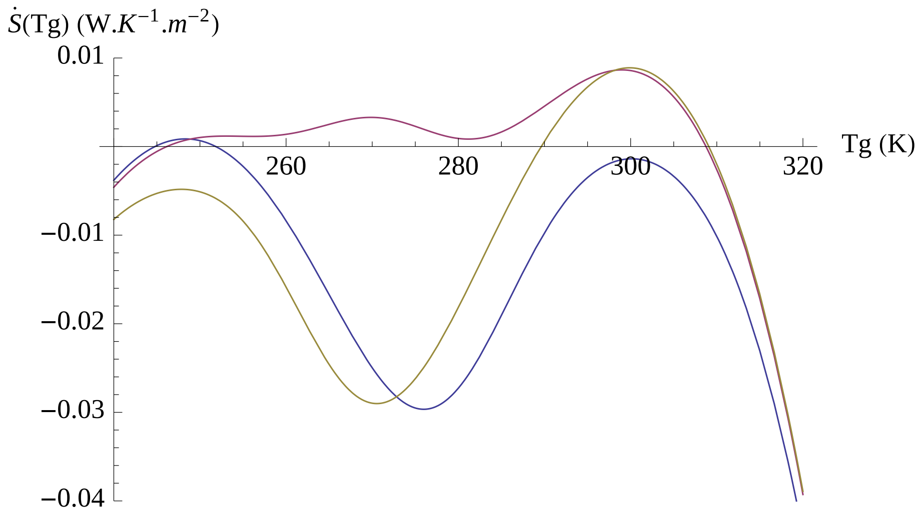

Fig. 7. Entropy production rate as a function of the surface temperature T_g for the 0D model with ice-albedo feedback. For a low value of the solar constant ($S = 0.8\,S_0$, blue curve), there is only one local maximum with positive entropy production rate. The same holds for high solar constant ($S = 1.2\,S_0$, yellow curve), while there are three local maxima and two minima, all with positive entropy production rates, for $S = S_0$ (red curve).

ESDD
1, 325–355, 2010

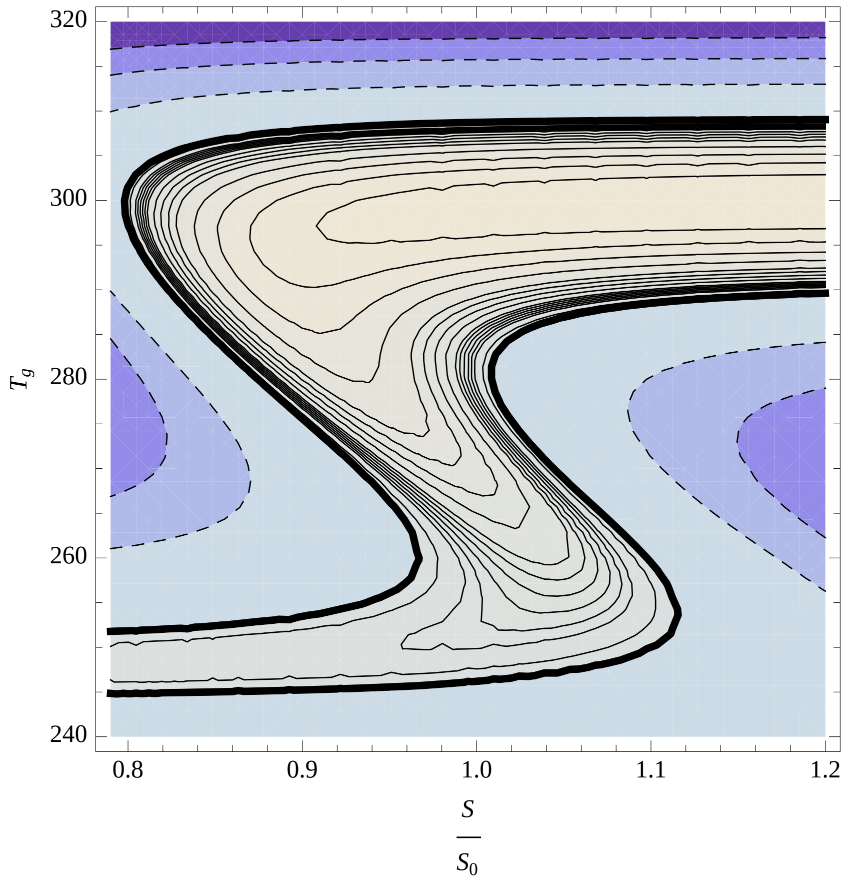

Fig. 8. Contour plot of the entropy production rate as a function of the solar constant (normalized by its present-day value) and the surface temperature T_g (in K). Negative contour lines are dashed, positive contour lines are solid and the null contour line is the thick solid line. Shades of blue represent negative values of the entropy production rate.

ESDD
1, 325–355, 2010

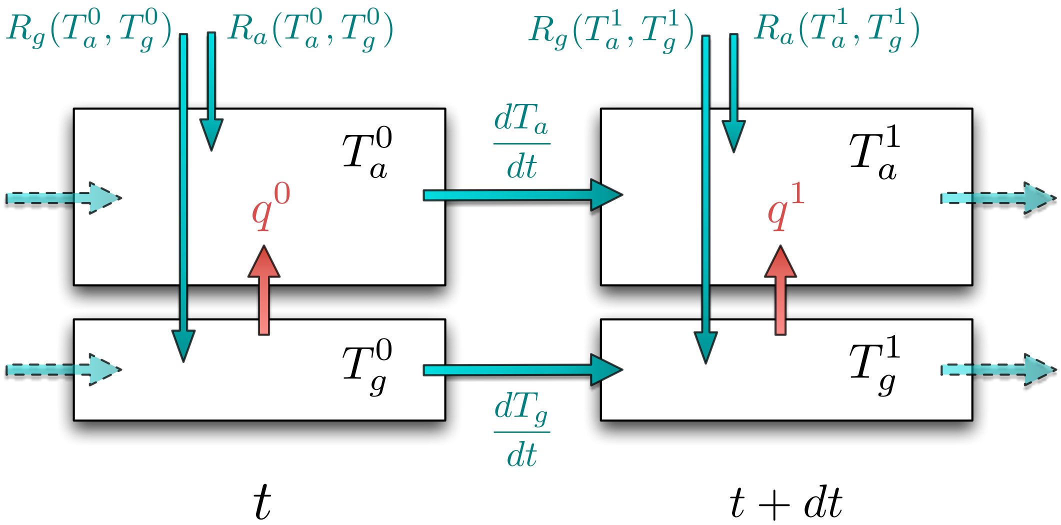

Fig. 9. To discuss the stability of the steady states predicted by MEP, we need to extend the principle to obtain a time-dependent formulation. This is done by considering that the time derivative of the temperature acts as a flux in time seen as a geometric dimension of the space upon which MEP operates. In green, the fluxes that can be computed from the state variables $\left(T_a^0, T_a^1, T_g^0, T_g^1\right)$. In red, the unknown fluxes obeying MEP.

ESDD
1, 325–355, 2010

Entropy production and the ice-albedo feedback

C. Herbert et al.

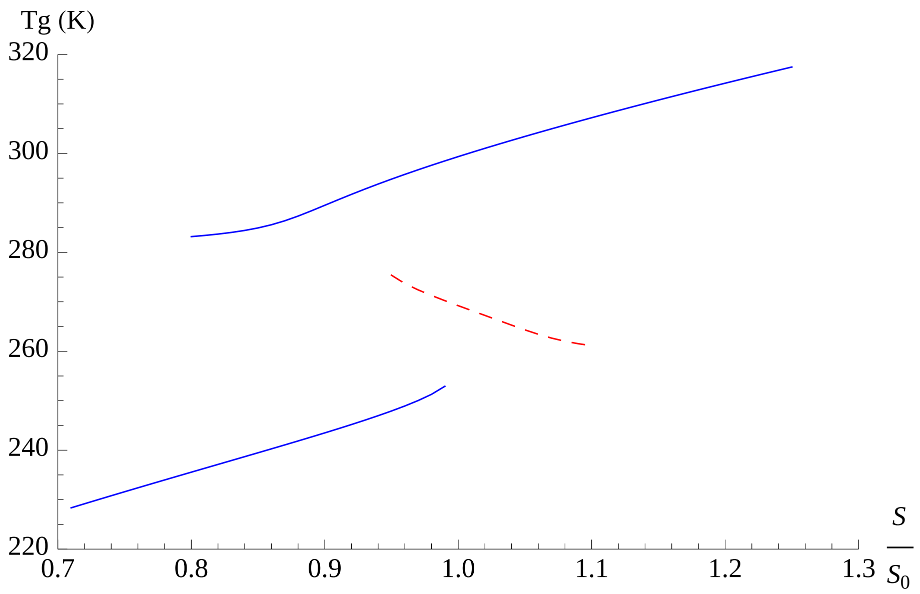

Fig. 10. Entropy Production maxima as a function of the solar constant, normalized by its present value. The solid lines (resp. the dotted line) correspond to dynamically stable (resp. unstable) equilibria in the sense of Sect. 3.2. Note that this is not a bifurcation diagram in the usual meaning.

ESDD
1, 325–355, 2010

Entropy production and the ice-albedo feedback

C. Herbert et al.

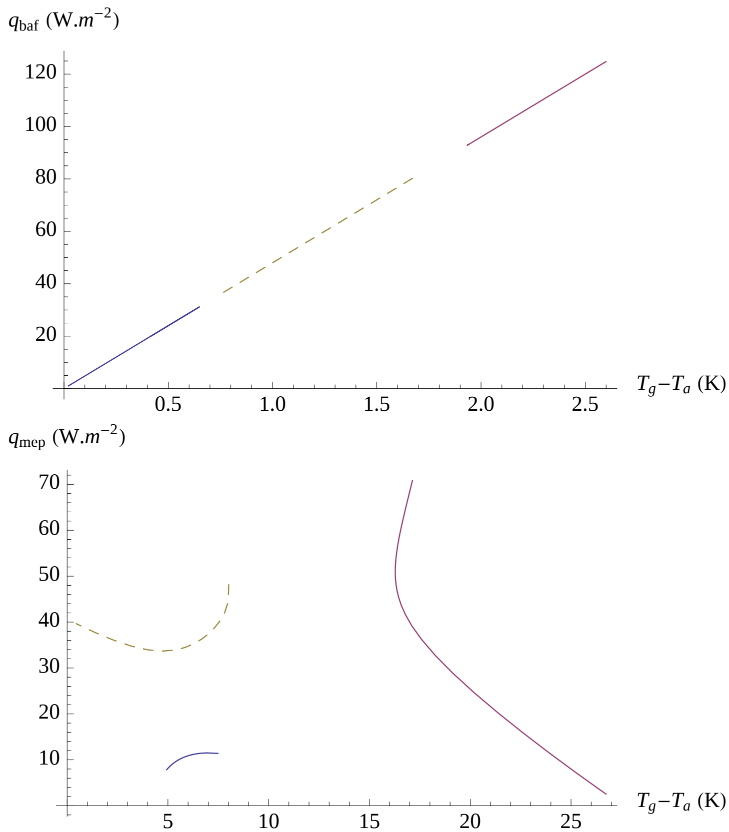

Fig. 11. Comparison between the bulk aerodynamic formula surface heat flux (top) and the MEP predicted surface heat flux (bottom) as a function of the temperature gradient $T_g - T_a$. The red solid line corresponds to the warm branch of the bifurcation diagram, the blue solid line to the snowball state and the dotted yellow line is the unstable branch. Note the very different scales for $T_g - T_a$.

ESDD
1, 325–355, 2010